

Physics

Physics Research Publications

Purdue University

Year 2010

Guard Ring Simulations for n-on-p
Silicon Particle Detectors

O. Koybasi

G. Bolla

D. Bortoletto

This paper is posted at Purdue e-Pubs.

http://docs.lib.purdue.edu/physics_articles/1272

Guard Ring Simulations for n-on-p Silicon Particle Detectors

Ozhan Koybasi, Gino Bolla, and Daniela Bortoletto

Abstract—We propose a new guard ring geometry for n-on-p silicon particle detectors for high luminosity applications. The performance of the guard ring structure is evaluated with simulations up to a radiation fluence of 1×10^{15} n_{eq}/cm² using an existing three level trap model for p-type FZ silicon. The post-irradiation performance improvement of guard rings with floating field plates pointing towards the sensitive region is demonstrated. The breakdown behavior of the guard ring structure is studied as a function of oxide charge, field plate length, and oxide thickness.

Index Terms—Device simulations, field plates, guard rings, n-on-p silicon particle detectors, radiation hardness.

I. INTRODUCTION

SILICON microstrip and pixel detectors used in the trackers of high luminosity collider experiments are exposed to charged particles (which cause ionizing displacement damages) with very high fluences due to their proximity to the interaction point. The displacement damage induces defects in the silicon crystal, leading to higher depletion voltages. Therefore, the tracking devices must be operated at high voltages to maintain full depletion or at least partial depletion of the substantial part of the detector volume, which is required to get a reasonable signal to noise ratio from the detector. The heavily damaged cutting edge of the sensor is a region of high generation and recombination and it may cause the leakage current to increase by orders of magnitude if the depletion region of the sensor extends to this edge. Furthermore, the positive oxide charge which increases with radiation induces a conductive electron channel at the silicon/oxide interface. Guard rings are needed to shield the sensitive region from the silicon surface and dice line leakage currents. The guard ring geometry should also establish a uniform potential drop along the silicon surface to avoid large potential drops over very short distances that may lead to local breakdowns at voltages much lower than the bias voltage required for detector operation.

In earlier times, almost all the developments in silicon detector technology for high energy physics were made using

n-type substrate with only a few on p-type silicon [1]. However, in last few years, p-type silicon as sensor material has shown promising results for radiation hardness [2]–[5] and it is now considered as a strong candidate among the scientific community to reduce the detrimental effects due to the harsh radiation environment. One advantage of the n-on-p sensor technology over the more conventional p-on-n one is that it collects electrons which have slightly larger trapping time and higher mobility in silicon compared to holes. Also, it has been demonstrated that during annealing, the trapping times increase for electrons and decrease for holes [6]–[8]. In the p-on-n geometry, the junction moves to the back-side after space charge sign inversion (SCSI) caused by radiation-induced negative space charges and, therefore, the high electric field is on the side opposite to the readout electrodes. If the detector is operated at partial depletion, the holes deposited in the depletion region spread over many readout electrodes due to the low electric field near the front surface, resulting in a degraded resolution. On the other hand, the junction is always located on the readout-side in n-on-p sensors due to non-SCSI, so it is not necessary to fully deplete the sensor to create a high electric field underneath the readout electrodes. In the n-on-n configuration, the collected carriers are also electrons and it has already been shown with extensive studies that these sensors are substantially more radiation hard than the p-on-n technology [5]. However, this approach is the most expensive one as it requires double-side processing, which makes the n-on-p technology extremely appealing. Further discussions on these different planar detector technologies can be found in [9].

Although numerous studies on guard ring designs for p-on-n and n-on-n silicon sensors can be found in the literature [10]–[16], no standard guard ring design for the relatively new n-on-p technology has been established yet. Recently, a preliminary study on the simulation of n-on-p guard rings for the ATLAS upgrade has been reported [17]. In this paper, we take a more thorough approach and investigate the impact of all design parameters with electrical simulations to develop an optimum guard ring structure for high voltage operation of n-on-p silicon detectors at high fluences for the upgrade of the LHC trackers. The proposed designs and some test structures dedicated for systematic comparison of experimental behavior with simulations will be implemented along with the CMS pixel sensors at SINTEF, Norway. Although no experimental data to validate the simulation results of the guard ring structures exist yet, simulations with the same tools and models were able to predict the experimentally observed breakdown behavior of different devices, namely 3D CMS pixel detectors, with a satisfactory accuracy. For 4-electrode (4E) and 2-electrode (2E) 3D CMS pixel sensors that have actual breakdown voltages of

Manuscript received December 15, 2009; revised April 21, 2010 and July 19, 2010; accepted July 26, 2010. Date of current version October 15, 2010. This work was supported in part by the U.S. Department of Energy under Grant DE-FG02-91ER40681 and in part by the National Science Foundation under Cooperative Agreement PHY 0612805 – UCLA Subaward 1000 G HD870.

O. Koybasi is with the Department of Physics and Birck Nanotechnology Center, Purdue University, West Lafayette, IN 47907 USA (e-mail: okoybasi@purdue.edu).

G. Bolla and D. Bortoletto are with the Department of Physics, Purdue University, West Lafayette, IN 47907 USA (e-mail: gino.bolla@cern.ch; bortolet@purdue.edu).

Color versions of one or more of the figures in this paper are available online at <http://ieeexplore.ieee.org>.

Digital Object Identifier 10.1109/TNS.2010.2063439

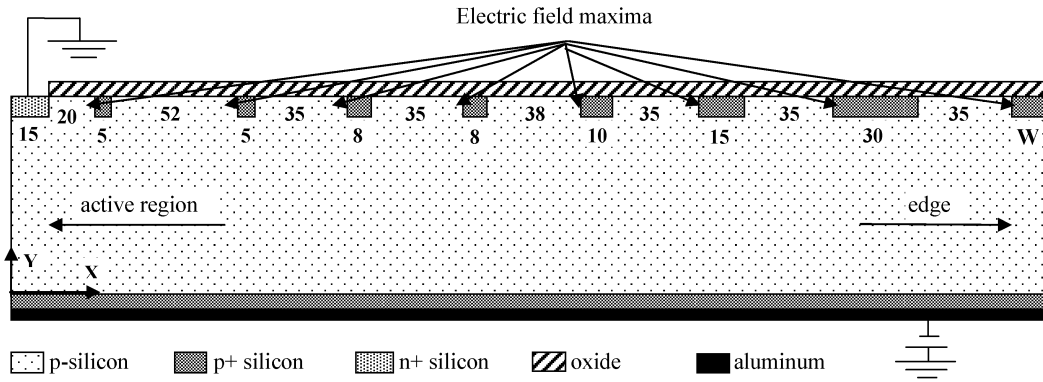


Fig. 1. Optimum guard ring structure for an oxide charge of $4 \times 10^{11} \text{ cm}^{-2}$.

$\sim 85 \text{ V}$ and $\sim 110 \text{ V}$, respectively, the corresponding simulated breakdown voltages are $\sim 80 \text{ V}$ and $\sim 95 \text{ V}$ [18].

The simulations have been performed with Synopsys Sentaurus TCAD [19] which is a 1D/2D/3D finite element semiconductor simulation package capable of simulating the processing and electrical, thermal, and optical characteristics of semiconductor devices made with various semiconductor materials. Sentaurus Device takes a mesh made of discrete elements as an input structure and solves the Poisson's equation along with carrier continuity equations at every grid point on the mesh to calculate the electrical properties such as current and capacitance and physical quantities such as carrier distribution, carrier mobility and potential distribution inside the semiconductor. In addition to electron, hole, acceptor, and donor charges, the Poisson's equation takes into consideration the charges associated with radiation-induced trap levels. The dynamic behavior of traps is described by Shockley Read Hall recombination which depends on trap concentration, energy, and carrier cross sections. Doping dependent mobility degradation, mobility saturation at high fields and mobility degradation at interfaces were taken into account with the mobility models used. The physical models employed in the simulation include band gap narrowing at high doping concentration and high temperatures as well. Sentaurus has several models that can be activated to simulate the impact ionization which is the free carrier generation mechanism leading to avalanche breakdown. The impact ionization model suggested by Okuto and Crowell [20] was used to evaluate the breakdown behavior of the guard ring structure. Since the length of guard rings is quite large compared with the substrate thickness and the width of the sensor periphery, simulations over a 2D cross section orthogonal to the length of guard rings can provide accurate enough information regarding the 3D guard ring behavior. The mesh was refined near the silicon/oxide interface with a maximum height of $0.15 \mu\text{m}$ and width of $0.8 \mu\text{m}$ to improve the accuracy of the results although a convergence study has shown that the breakdown voltage does not vary with mesh refinement near the silicon/oxide interface.

II. SIMULATION WITH NO RADIATION DAMAGE

Fig. 1 shows the 2D cross section of the seven p+ guard ring structure used in the simulation, optimized for an oxide charge of $4 \times 10^{11} \text{ cm}^{-2}$. The simulations were carried out

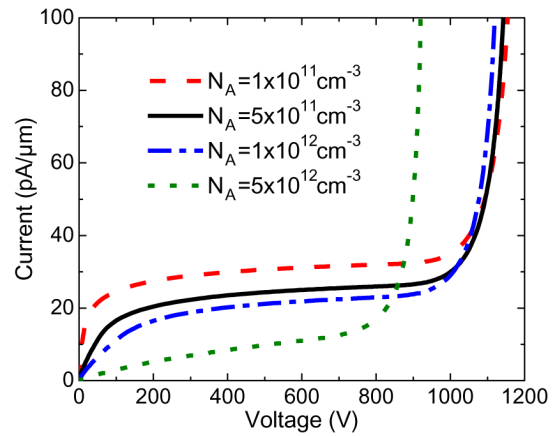


Fig. 2. Leakage current versus reverse bias voltage as a function of substrate doping concentration for the guard ring structure in Fig. 1.

with a substrate thickness of $300 \mu\text{m}$ and substrate doping of $5 \times 10^{11} \text{ cm}^{-3}$. Although the substrate doping concentration and the doping profile of the guard rings do not play a role in determining the optimum guard ring geometry as long as they are within the range of typical values, the breakdown voltage for a given geometry is influenced by these parameters. Therefore, it is worth investigating how the breakdown of the guard ring structure changes with substrate and guard ring doping before discussing the impact of other parameters on the design.

Leakage current versus reverse bias voltage characteristics of the guard ring structure in Fig. 1 with four different substrate doping concentrations is shown in Fig. 2. As one would expect, the substrate with the highest resistivity yields the highest breakdown voltage (the reverse bias voltage at which the leakage current starts to rise exponentially). However, although the breakdown increases considerably (by $\sim 200 \text{ V}$) when the substrate doping is reduced from $5 \times 10^{12} \text{ cm}^{-3}$ to $1 \times 10^{12} \text{ cm}^{-3}$, it varies very slightly over the range of substrate doping concentration from $1 \times 10^{12} \text{ cm}^{-3}$ to $1 \times 10^{11} \text{ cm}^{-3}$. Higher substrate resistivity is desired since it also leads to a lower depletion voltage even though it requires the inactive portion of the sensor to be larger as it will be discussed later. The increase of leakage current with lower substrate doping is attributed to the increasing depleted volume for an applied bias voltage, which is also true after the full-depletion (across substrate thickness) at

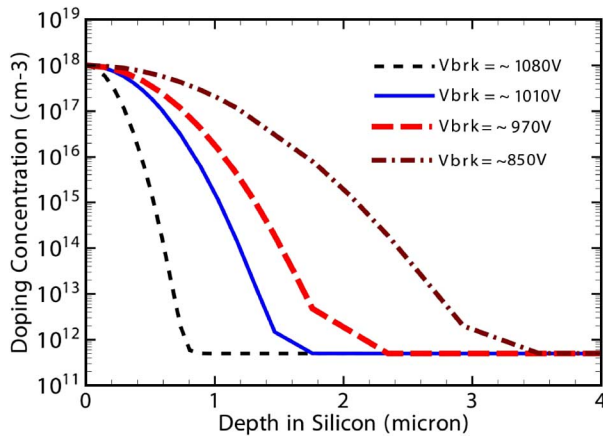


Fig. 3. Different p+ doping profile depths and corresponding breakdown voltages.

all doping levels is attained due to the lateral depletion towards the detector edge.

The effect of the guard ring doping profile has been investigated as follows.

- i) The peak guard ring doping concentration is kept at a constant value and the depth of the profile is varied.
- ii) The depth of the profile is fixed and the peak doping of guard rings is changed.

Fig. 3 suggests that the doping profile should be as shallow as possible. A breakdown voltage of ~ 1080 V has been achieved with a profile depth of $\sim 0.8 \mu\text{m}$ while it drops to ~ 850 V for a profile depth of $3.5 \mu\text{m}$. This is a remarkable observation as one would expect a deeper implant, which has a smaller curvature, to lead to a lower electric field and consequently a higher breakdown voltage. Indeed, the maximum electric field in silicon remains lower for structures with deeper implants up to voltages close to the start of impact ionization, after which the maximum electric field increases with a higher slope as a function of bias voltage. The deeper the implant, the lower the bias voltage at which the electric field changes slope. In this case, the guard ring design with a deeper implant reaches the electric field value that initiates the breakdown at lower voltages. In [21], it has been demonstrated that the breakdown voltage increases with strip implant depth for a p-on-n strip detector, and the same trend has been reproduced with our simulation tools and models. The only difference between the two situations is that the p+ implants are biased in the strip detector case while they are floating in the guard ring case. Deeper biased strips lead to a lower electric field due to smaller implant curvature and this trend persists up to the realization of the breakdown unlike floating guard rings in which the maximum electric field changes slope and this change occurs at lower bias voltages for deeper implants as discussed previously. In conclusion, the breakdown voltage is enhanced with implant depth for biased implants whereas the opposite statement holds true in the case of floating implants.

According to Fig. 4, the breakdown voltage increases with decreasing peak p+ ring doping but the increase is not significant. The minimum doping of the p+ rings is limited by the maximum value that oxide charge may reach. Although it seems to yield a higher breakdown, a peak doping of $1 \times 10^{17} \text{ cm}^{-3}$ will not be

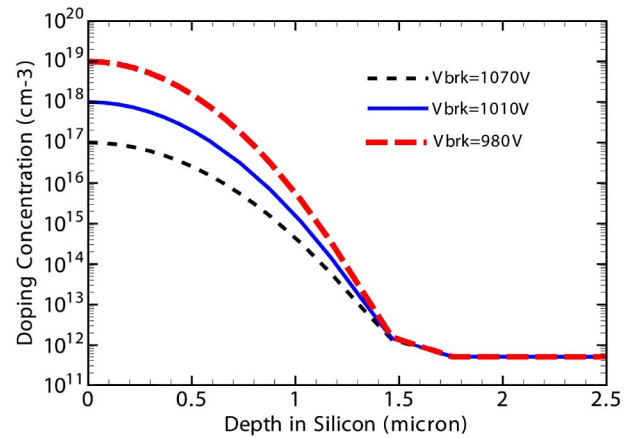


Fig. 4. Different values of peak p+ doping concentration and corresponding breakdown voltages.

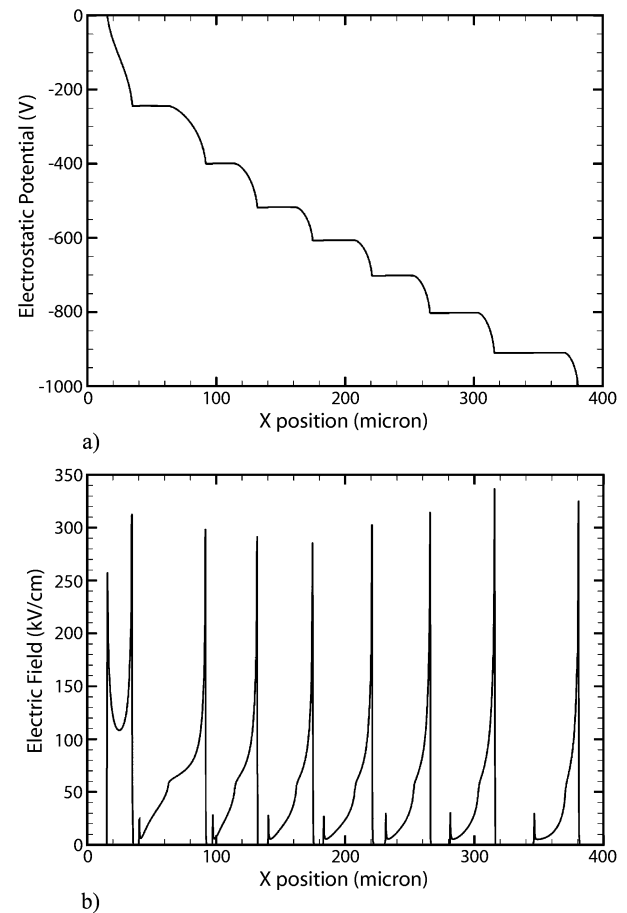


Fig. 5. a) Potential drop and b) electric field along a cut line parallel to the device surface at a depth of 100 nm from silicon/oxide interface for an oxide charge of $4 \times 10^{11} \text{ cm}^{-2}$.

sufficiently high to compensate the surface channel if the oxide charge reaches up to $3 \times 10^{12} \text{ cm}^{-3}$. This value of oxide charge requires a peak p+ ring doping of at least $\sim 5 \times 10^{17} \text{ cm}^{-3}$ to prevent surface charge from inversion.

In Fig. 1, the width of p+ guard rings and the spacing between them have been set in such a way that equal amount of potential drop occurs at each guard ring. This makes the corresponding electric field peaks more or less the same, minimizing

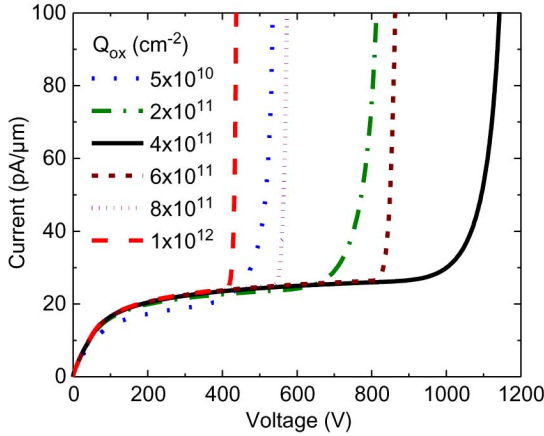
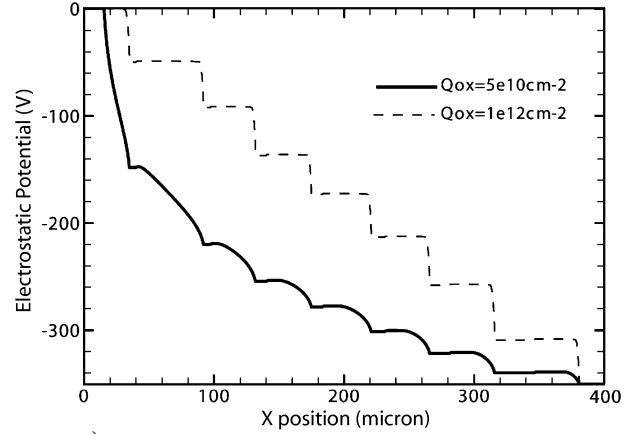


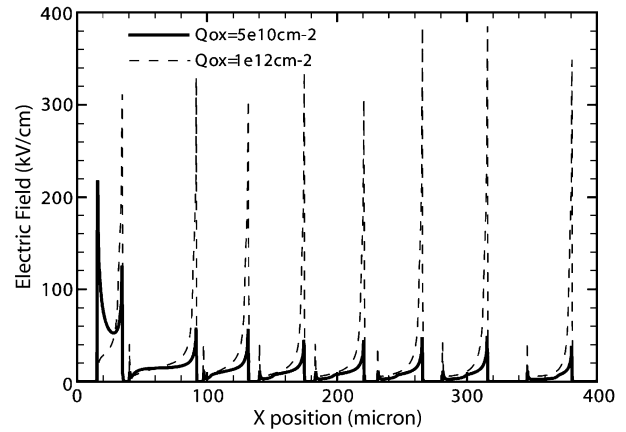
Fig. 6. Leakage current versus reverse bias voltage for different values of oxide charge. The decrease in breakdown voltage at oxide charges lower than $4 \times 10^{11} \text{ cm}^{-2}$ is due to the non-uniform distribution of potential along the guard rings while at oxide charge higher than $4 \times 10^{11} \text{ cm}^{-2}$ it is mainly due to more abrupt potential drop at each guard ring.

the maximum electric field throughout the entire structure. In optimizing the geometry, a fixed oxide charge of $4 \times 10^{11} \text{ cm}^{-2}$ was assumed. The electric field maxima are located at the lateral p-/p+ boundaries facing the diode where the electron channel is interrupted and the potential drops. Fig. 5 shows the potential drop and the corresponding electric field distribution along the detector surface at a depth of 100 nm from the silicon/oxide interface. With this potential distribution, the device is able to sustain reverse biases exceeding 1000 V as shown in Fig. 6. For lower or higher values of oxide charge, the guard ring performance degrades significantly. The breakdown voltage decreases as the deviation of oxide charge from $4 \times 10^{11} \text{ cm}^{-2}$ increases. At low oxide charges, since silicon surface conductivity is low, the majority of the potential drops at the diode and innermost guard rings. The potential drops more evenly at all guard rings with increasing surface conductivity. This goes in parallel with an increasing slope of potential drop at each guard ring. After a very uniform field distribution is reached at an oxide charge of $4 \times 10^{11} \text{ cm}^{-2}$, further increase in oxide charge makes the potential drop at each guard ring steeper due to increasing surface conductivity, resulting in higher electric field peaks and consequently lower breakdown voltage. Fig. 7 shows the potential drop and the corresponding electric field for two extreme values of oxide charge, $5 \times 10^{10} \text{ cm}^{-2}$ and $1 \times 10^{12} \text{ cm}^{-2}$, at a reverse bias voltage of 350 V which is just below the breakdown. Note that the uniformity of potential distribution does not change significantly with further increase in oxide charge once it becomes even for a certain oxide charge. Therefore, if the guard ring structure needs to be optimized for higher values of oxide charge, this cannot be accomplished by only modifying the width of guard rings and the spacing between them but it also requires the number of guard rings to be increased. In this case, the applied bias voltage will be shared between more guard rings, resulting in less potential drop and a lower electric field at each guard ring.

Since the area under the oxide is already n+ due to the positive oxide charge, adding n+ guard rings does not affect the potential distribution and therefore the breakdown behavior. This



a)



b)

Fig. 7. a) Potential drop and b) electric field along a cut line parallel to the device surface at a depth of 100 nm from silicon/oxide interface for oxide charges of $5 \times 10^{10} \text{ cm}^{-2}$ and $1 \times 10^{12} \text{ cm}^{-2}$. The detector is reverse biased at 350 V which is just below the breakdown voltage.

was also confirmed with simulation. However, one n+ guard ring between the sensitive region and the innermost p+ guard ring is needed for biasing to the ground potential to make the field uniform near the outermost pixel/strip.

When the sensor is reverse-biased, the depletion region spreads out laterally from the p-n junction toward the cutting edge of the sensor. If the space charge region reaches out to the edge which is a very effective generation center due to crystal damage caused by cutting, charge is injected into the depleted zone from the scribe line, increasing the leakage current. In order to prevent the depletion region from reaching the edge, the surface of the sensor periphery must be terminated by a wide p+ implant whose width is denoted by W in Fig. 1. The minimum W required to prevent the depletion region from making contact with the cutting edge at reverse biases of 1000 V and V_{DEP} (bias voltage required for full depletion) has been simulated for different values of substrate doping. The results are presented in Table I. For the guard ring structure, the depletion voltages associated with each substrate doping are higher than those for an un-structured diode, which would be 7 V, 35 V, and 70 V for substrate doping of $1 \times 10^{11} \text{ cm}^{-3}$, $5 \times 10^{11} \text{ cm}^{-3}$, $1 \times 10^{12} \text{ cm}^{-3}$, respectively. This is because of the lateral depletion of the guard ring structure as well as the traversal depletion.

TABLE I
W AS A FUNCTION OF SUBSTRATE DOPING AT BIASES OF 1000 V AND V_{DEP}

N_A (cm ⁻³)	W at 1000 V (μm)	V_{DEP} (V)	W at V_{DEP} (μm)
1×10^{11}	390	260	290
5×10^{11}	250	300	160
1×10^{12}	185	350	105

N_A , W, and V_{dep} represent the substrate doping, minimum outermost p+ width, and depletion voltage, respectively.

III. SIMULATIONS WITH RADIATION DAMAGE

The incident radiation creates defects in the silicon lattice, forming extra energy levels in the band gap of silicon that act as generation-recombination and charge trapping centers. The primary effects of these bulk traps are

- i) an increase in leakage current proportional to the radiation fluence:

$$\Delta I/V = \alpha\varphi \quad (1)$$

where V is the depleted volume, φ is the fluence, and α is the damage rate constant;

- ii) an increase in depletion voltage due to increasing effective doping concentration (N_{eff}):

$$V_{\text{dep}} \cong qN_{\text{eff}}d^2/2\varepsilon_0K_{\text{si}} \quad (2)$$

where q is the electronic charge, d is the substrate thickness, ε_0 is the permittivity of free space, and K_{si} is the dielectric constant of silicon;

- iii) a decrease in charge collection efficiency due to increasing carrier trapping.

In addition to the displacement damage that introduces bulk-defects, the ionizing radiation by charged particles also gives rise to an increase in positive oxide charge near the silicon/oxide interface. A part of the ionizing radiation-generated carriers in the oxide recombine immediately while the surviving electrons and holes drift in opposite directions under the effect of the oxide field. Since the electrons have a relatively high mobility in SiO_2 ($\approx 20 \text{ cm}^2/\text{V}\cdot\text{s}$), they are quickly swept out of the oxide. The holes, on the other hand, have a very low mobility in the SiO_2 ($\approx 2 \times 10^{-5} \text{ cm}^2/\text{V}\cdot\text{s}$) due to numerous shallow hole traps that exist in the oxide. The holes move very slowly in direction of oxide field from one shallow trap to another and when they reach the silicon/oxide interface, where many deep hole traps exist, they either recombine with electrons from silicon or get trapped there permanently. The overall effect is an increase in the oxide charge. This increase is not an everlasting process and the oxide charge saturates at densities up to a few 10^{12} cm^{-2} after a radiation dose of some kilograys due to the finite number of existing traps. In [22], it has been observed that the oxide charge saturates at $\sim 1.5 \times 10^{12} \text{ cm}^{-2}$ for p-type FZ and MCz silicon with $\langle 100 \rangle$ surface orientation and at $\sim 2.0 \times 10^{12} \text{ cm}^{-2}$ for n-type FZ silicon with $\langle 111 \rangle$ surface orientation after a radiation dose of 150 krad whereas [23] claims a saturation value

TABLE II
THE UNIVERSITY OF PERUGIA TRAP MODEL

Type	Energy (eV)	Trap	σ_e (cm ²)	σ_h (cm ²)	η (cm ⁻¹)
Acceptor	$E_C-0.42$	VV	2.0×10^{-15}	2.0×10^{-14}	1.613
Acceptor	$E_C-0.46$	VVV	5.0×10^{-15}	5.0×10^{-14}	0.9
Donor	$E_V+0.36$	CiOi	2.5×10^{-14}	2.5×10^{-15}	0.9

of $1 \times 10^{12} \text{ cm}^{-2}$, and some older references such as [24] have reported a value of $3 \times 10^{12} \text{ cm}^{-2}$.

A trap model has been proposed by the University of Perugia [23] to describe radiation damage caused by proton irradiation in p-type FZ silicon. According to the model, the radiation generates two acceptor levels positioned slightly above the mid band gap and one donor level located far below the mid band gap. The details of the trap model are presented in Table II. Since the acceptor states are close to the mid band gap, they will generate electron-hole pairs, increasing the leakage current. A small portion of the acceptor states will be occupied and therefore negatively charged, increasing the effective p-type doping while the unoccupied acceptor states will trap excess electrons in the conduction band. The function of the donor state, which is far below the mid band gap, is to trap excess holes from the valence band.

This trap model accurately predicts the increase in leakage current and effective doping concentration due to irradiation but not the trapping behavior. The carrier cross sections in this model have been modified at University of Glasgow to accurately predict the trapping rates [25]. As long as the ratio of electron cross section σ_e to hole cross section σ_h is constant, the depletion voltage changes very slightly with altering each cross section. Therefore, the carrier cross sections have been modified in such a way that they yield trapping rates that match the experimental data but at the same time the σ_e/σ_h ratio is kept constant not to impact the effective doping concentration which is predicted accurately by the University of Perugia model. The parameters of the modified model are shown in Table III. This model yields a current-related damage rate of $\alpha = 5.13 \times 10^{-17} \text{ Acm}^{-1}$ which is about 30% higher than the experimental value of $\alpha = 3.99 \pm 0.03 \times 10^{-17} \text{ Acm}^{-1}$ as measured at 293 K after an 80 minute annealing at 60°C [26]. The leakage current can change by more than 30% under different annealing conditions. If the aim of the simulation is to model the effective doping concentration and trapping behavior rather than the amount of leakage current, the model seems to work quite well. For guard ring simulations, only the change in effective doping concentration is relevant so either radiation damage model can be used.

The post irradiation performance of the guard ring structure has been evaluated with simulations using the modified trap model in Table III. Fig. 8 and Fig. 9 show the breakdown behavior of the guard ring structure after irradiation for different values of fluence and oxide charge, respectively. The breakdown behavior degrades significantly with irradiation. For an oxide charge of $1 \times 10^{12} \text{ cm}^{-2}$, the structure is able to survive only

TABLE III
 THE MODIFIED VERSION OF THE UNIVERSITY OF PERUGIA TRAP MODEL

Type	Energy (eV)	Trap	σ_c (cm ²)	σ_h (cm ²)	η (cm ⁻¹)
Acceptor	$E_C-0.42$	VV	9.5×10^{-15}	9.5×10^{-14}	1.613
Acceptor	$E_C-0.46$	VVV	5.0×10^{-15}	5.0×10^{-14}	0.9
Donor	$E_V+0.36$	CIoI	3.23×10^{-13}	3.23×10^{-14}	0.9

The modified parameters are shown in bold.

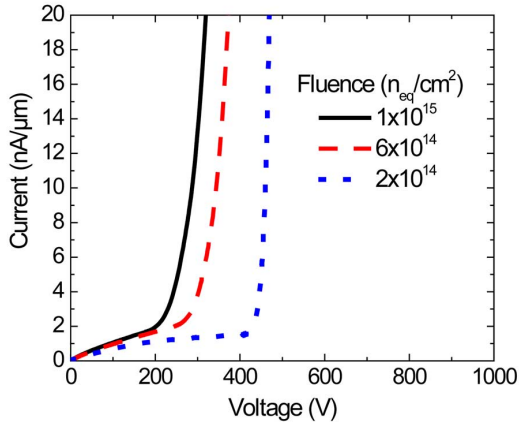


Fig. 8. Leakage current versus reverse bias voltage at different fluences. The oxide charge is 1×10^{12} cm⁻².

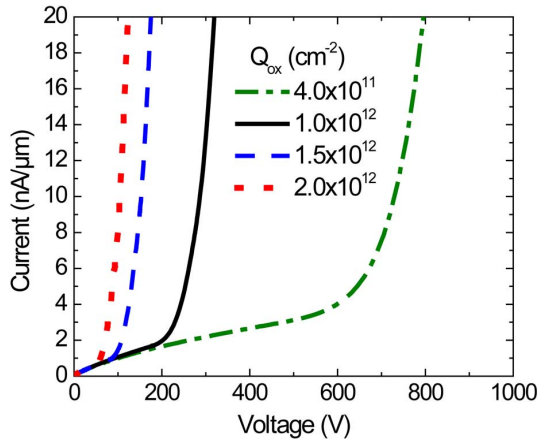


Fig. 9. Leakage current versus reverse bias voltage for different values of oxide charge after a radiation fluence of 1×10^{15} n_{eq}/cm².

up to reverse biases of ~ 200 V at a fluence of 1×10^{15} n_{eq}/cm² while the breakdown voltage is as low as 50 V when the oxide charge rises to 2×10^{12} cm⁻² at the same fluence. The decrease in breakdown voltage after irradiation is attributed to two reasons.

- i) Due to increasing surface conductivity as a consequence of increasing oxide charge, the potential drop at each p+ guard ring becomes steeper, resulting in higher electric fields.
- ii) Depletion voltage increases due to the radiation-induced bulk traps. Therefore, for a given applied bias, the volume of space charge region decreases with irradiation and all

potential drops at the inner guard rings since the depletion region does not reach the outer ones.

The breakdown voltages in Fig. 8 and Fig. 9 are not high enough for very high luminosity applications, so further improvements are needed.

A. Field Plates

The electric field after irradiation can be reduced by using field plates pointing towards the sensitive region as depicted in Fig. 10. The field plates are at the potential of the silicon regions they are in contact with. Therefore, in this configuration, they are at lower potential than the underlying silicon as the potential drops from the active region towards the edge. This forms a negatively biased p-bulk MOS structure, which may result in depletion of free carriers from the silicon surface or accumulation of holes at the silicon/oxide interface, depending on the flat band voltage and potential difference between the field plates and the underlying silicon. Fig. 11 shows the electron density and electric field distribution around the two innermost guard rings of the optimized sensor periphery with field plates at a reverse bias of 900 V for a radiation fluence of 1×10^{15} n_{eq}/cm² and an oxide charge of 1×10^{12} cm⁻². The electron layer disappears at the silicon/oxide interface regions underneath the portion of the field plates on the left of the p+ rings due to the lower electrostatic potential of the field plates with respect to the silicon surface. With the use of field plates, the potential drop starts underneath the left edges of the field plates where secondary electric field peaks in silicon are formed in addition to the ones at the p-/p+ boundary facing the active region while the highest field spots over all the structure are located in the oxide due to the large potential difference across its thickness. The breakdown voltage improves with the creation of secondary electric field peaks since the electric field will be distributed over more spots with a lower peak value at each spot.

The n+ guard rings in Fig. 10 are used for the contact of the field plates to the silicon. In principle, it would be possible to make these contacts on the p+ guard rings if they were wide enough, which would give the same potential distribution. However, the inner p+ rings are too narrow to put the metal contacts on (according to SINTEF design rules) and increasing their width will change the potential distribution in silicon. That is why n+ rings, which have no effect on potential distribution, are used for metal contacts. Indeed, the three outermost p+ rings are wide enough to be used for metal contact and an alternative structure that gives identical performance would be one with the outer three field plates in contact with the p+ rings instead the n+ rings next to them. If the field plates extend outwards, the electric field is not reduced since the field plates will be at the same potential as the underlying silicon between the contact n+ ring and the p+ ring on its right, and a higher potential than the underlying silicon at the location of the p+ ring and beyond, which causes further build of electron layer at the interface of SiO₂ and Si.

The simulation of the breakdown behavior of the guard ring structure with field plates as a function of radiation fluence is shown in Fig. 12. With the assumption that the oxide charge saturates at 1×10^{12} cm⁻², a breakdown voltages of ~ 900 V,

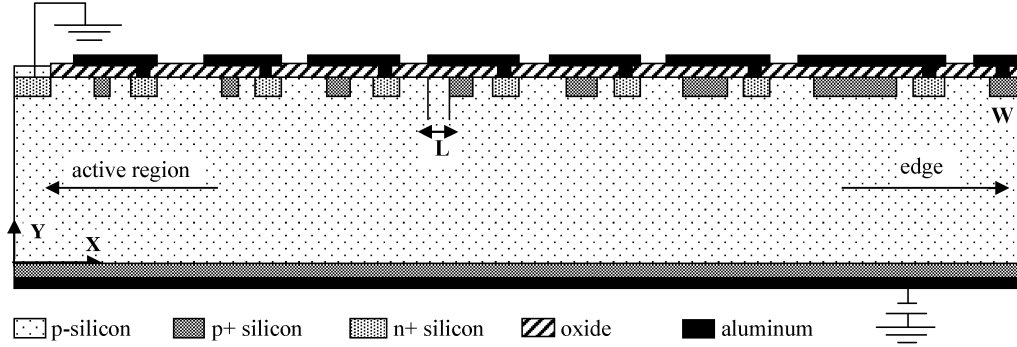


Fig. 10. Guard ring structure featuring field plates extending towards the sensitive region. The width and spacing of p+ guard rings are identical to those in Fig. 1.

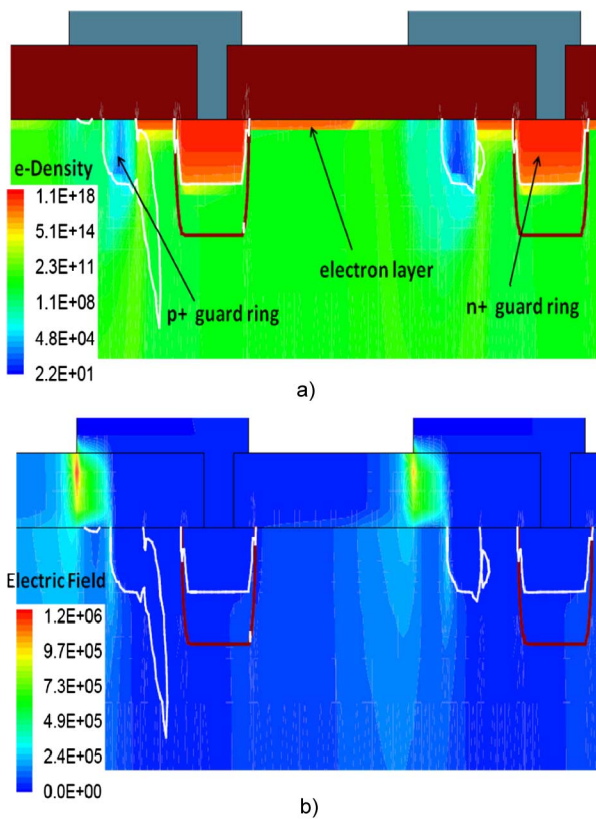


Fig. 11. a) Electron density distribution (in cm^{-3}) and b) electric field distribution (in V/cm) around the two innermost guard rings. The oxide charge is $1 \times 10^{12} \text{ cm}^{-2}$ and oxide thickness is $1 \mu\text{m}$. The ratio of the horizontal scale to vertical scale is 1/10. The white and brown lines represent the boundary of the depletion region and the interface of p-type and n-type regions, respectively.

$\sim 1100 \text{ V}$, and $\sim 1400 \text{ V}$ have been attained after fluences of $1 \times 10^{15} \text{ n}_{\text{eq}}/\text{cm}^2$, $6 \times 10^{14} \text{ n}_{\text{eq}}/\text{cm}^2$, and $2 \times 10^{14} \text{ n}_{\text{eq}}/\text{cm}^2$, respectively. Comparing with Fig. 9 which shows the simulation results for the same fluences in the absence of field plates, it can be seen that the breakdown voltage has been enhanced significantly with the use of field plates. Furthermore, $\sim 298 \mu\text{m}$ of the $300 \mu\text{m}$ substrate thickness is depleted before the breakdown at fluence of $1 \times 10^{15} \text{ n}_{\text{eq}}/\text{cm}^2$ while the detector reaches full depletion well below the breakdown for fluences of $2 \times 10^{14} \text{ n}_{\text{eq}}/\text{cm}^2$ and $6 \times 10^{14} \text{ n}_{\text{eq}}/\text{cm}^2$ as indicated by the simulation.

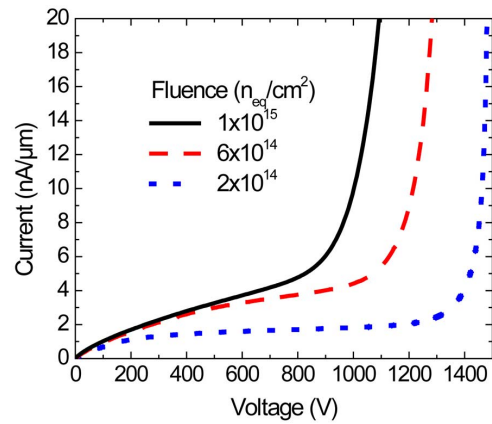


Fig. 12. Breakdown behavior of the guard ring structure with field plates as a function of radiation fluence. The oxide thickness is $1 \mu\text{m}$ and the field plate length, L , which is defined in Fig. 10 is $6 \mu\text{m}$. The oxide charge is assumed to saturate at $1 \times 10^{12} \text{ cm}^{-2}$.

B. Oxide Thickness

The flat band voltage depends on the thickness of the oxide between the field plates and silicon (t_{ox}) as well as the oxide charge (Q_{ox})

$$\Delta V_{\text{FB}} = qt_{\text{ox}}Q_{\text{ox}}/\epsilon_0 K_{\text{ox}} \quad (3)$$

where K_{ox} is the dielectric constant of SiO_2 . Therefore, the oxide thickness should play an important role in charge carrier distribution and consequently in breakdown voltage. Simulations with different oxide thicknesses were performed for various oxide charge densities as shown in Fig. 13. For the silicon regions underneath the field plates, only the product of oxide charge and oxide thickness affects the carrier distribution. However, for the silicon regions not covered with field plates, the oxide thickness does not matter and the oxide charge is the only parameter influencing the surface charge. For two devices having the same product of oxide thickness and oxide charge but different values of oxide charge and oxide thickness, the one with higher oxide charge density should have a lower breakdown voltage because the potential drop at the locations where electron channel is interrupted will be sharper. This explains why, for example, the breakdown voltage corresponding to an oxide thickness of $1.5 \mu\text{m}$ and oxide charge density of

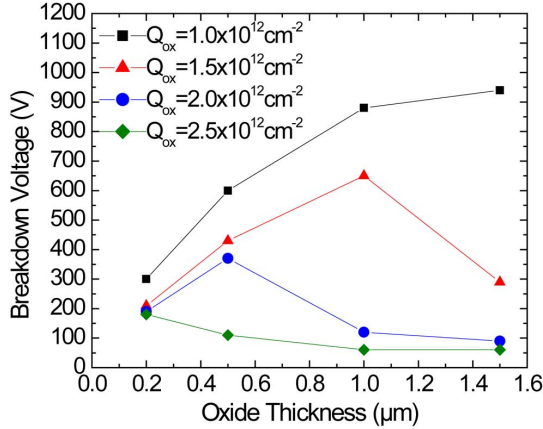


Fig. 13. Breakdown behavior as a function of oxide charge for different oxide thicknesses at a fluence of $1 \times 10^{15} \text{ n}_{eq}/\text{cm}^2$.

$1 \times 10^{12} \text{ cm}^{-2}$ is higher compared to the one corresponding to an oxide thickness of $1.0 \mu\text{m}$ and oxide charge density of $1.5 \times 10^{12} \text{ cm}^{-2}$ although they have the same $t_{ox}Q_{ox}$ product. As it can be seen in Fig. 13, the simulations indicate an optimum oxide thickness of $1.5 \mu\text{m}$ and $1 \mu\text{m}$ for oxide charge densities of $1 \times 10^{12} \text{ cm}^{-2}$ and $1.5 \times 10^{12} \text{ cm}^{-2}$, respectively, regarding breakdown voltage. For Q_{ox} equal to $2 \times 10^{12} \text{ cm}^{-2}$ the optimum thickness is $0.5 \mu\text{m}$ and for $2.5 \times 10^{12} \text{ cm}^{-2}$ the optimum is $0.2 \mu\text{m}$. Roughly speaking, it seems that, for a given Q_{ox} , as the deviation of the product of t_{ox} and Q_{ox} from $\sim 1 \mu\text{m} \times 10^{12} \text{ cm}^{-2}$ increases, the breakdown voltage decreases.

C. Field Plate Length

Obviously, the length of field plates influences the carrier distribution in silicon. Therefore, the optimum field plate length that yields the highest breakdown must be determined. The effect of the field plate length is investigated as a function of oxide charge for an oxide thickness of $1 \mu\text{m}$. Characterizing the field plate length by the distance L between the lateral boundary of the underlying p+ ring facing the p-n junction and the left end of the field plate as depicted in Fig. 10, the breakdown voltage versus field plate length for different oxide charges is shown in Fig. 14. The dependence of breakdown voltage on field plate length is non-monotonic. For oxide charges of $1 \times 10^{12} \text{ cm}^{-2}$ and $1.5 \times 10^{12} \text{ cm}^{-2}$, the breakdown voltage initially increases with field plate length as the maximum electric field spot at the p-/p+ boundary facing the active region decreases while the secondary electric field peak underneath the left edge of the field plate increases, and therefore, the electric field distribution over the two spots of the guard ring becomes more even. This trend continues up to field plate lengths of $4 \mu\text{m}$ and $5 \mu\text{m}$ for oxide charges of $1 \times 10^{12} \text{ cm}^{-2}$ and $1.5 \times 10^{12} \text{ cm}^{-2}$, respectively, with corresponding breakdown voltages of $\sim 980 \text{ V}$ and $\sim 680 \text{ V}$. The decrease of the breakdown voltage with further increase of the field plate length is a result of the changing uniformity of the electric field distribution over all guard rings as the amount of potential drop at a certain guard ring affects the potential distribution over the ones on its right. For oxide charge values of $2 \times 10^{12} \text{ cm}^{-2}$ and $2.5 \times 10^{12} \text{ cm}^{-2}$, it has been observed that

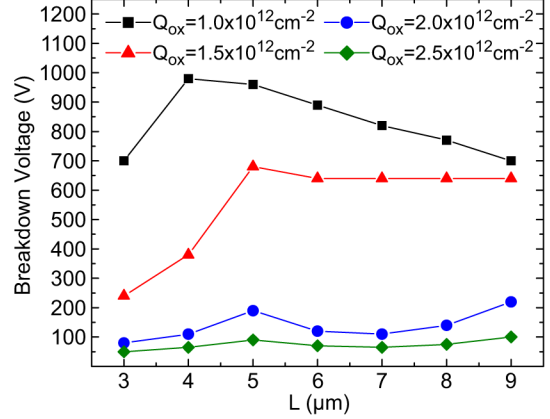


Fig. 14. Breakdown voltage versus field plate length as a function of oxide charge at a fluence of $1 \times 10^{15} \text{ n}_{eq}/\text{cm}^2$. The oxide thickness is $1 \mu\text{m}$.

the electron channel underneath the field plate is not compensated due to the large shift in flat band voltage to the more negative values with increasing oxide charge, so essentially no secondary electric field peak is formed underneath the field plate edge. The relatively small changes in breakdown voltage as a function of field plate length for these oxide charges are a consequence of the changes in the uniformity of electric field peaks at the p-/p+ boundaries facing the sensitive region. The breakdown voltages for the highest two values of oxide charge, which are below 250 V , can be enhanced by reducing the oxide thickness, and consequently, the shift in flat band voltage.

IV. CONCLUSIONS

Device simulations have shown that optimized guard rings without field plates can withstand reverse bias voltages above 1000 V without any radiation damage for an oxide charge of $4 \times 10^{11} \text{ cm}^{-2}$. A breakdown voltage above 900 V can be achieved with the proposed structure featuring field plates pointing toward the active region after a radiation fluence of $1 \times 10^{15} \text{ n}_{eq}/\text{cm}^2$, assuming the oxide charge saturates at a density of $1 \times 10^{12} \text{ cm}^{-2}$. However, for oxide charge values of $\sim 2 \times 10^{12} \text{ cm}^{-2}$ and above, the field plate solution to improve the breakdown after exposure to high ionizing radiation doses fails for an oxide thickness of $1 \mu\text{m}$ and the breakdown voltage decreases to below 250 V regardless of the field plate length. For the field plate solution to become effective for these values of oxide charge, the oxide thickness should be diminished to reduce the flat band voltage shift to such a value that the potential difference between field plate and underlying silicon can compensate the electron channel at the silicon/oxide interface. However, this will be at the expense of decreasing the breakdown voltage for lower oxide charges. Therefore, the road map for further optimization will be identified after measuring the saturated oxide charge density on the fabricated devices. Our future work will also address the optimization of guard rings (within the limits of design rules) for fluences above $1 \times 10^{15} \text{ n}_{eq}/\text{cm}^2$ to see the upper fluence limit at which these devices can be operated. Due to the lack of experimental data to support most of the simulation observations, test structures that feature different doping profiles, guard ring dimensions and spacing, field plate lengths, and oxide thicknesses will be

fabricated at SINTEF to confirm if the experimental behavior follows the same trend as the predictions of the simulation. In case of any offset between the simulation and experimental data, the parameters of the models will be tuned to improve the convergence of the theory to the measurement results.

ACKNOWLEDGMENT

The authors would like to thank T.-E. Hansen for helpful discussions.

REFERENCES

- [1] G. Bolla, D. Bortoletto, C. P. Grim, R. L. Lander, Z. Li, and S. Willard, "First results on radiation damage studies using n+/p/p+ diodes fabricated with multi-guard ring structures," *Nucl. Instrum. Meth. A*, vol. 435, pp. 178–186, 1999.
- [2] G. Casse, P. P. Allport, P. R. Turner, S. Marti i Garcia, and M. Lozano, "Performances of miniature microstrip detectors made on oxygen enriched p-type substrates after very high proton irradiation," *Nucl. Instrum. Meth. A*, vol. 535, pp. 362–365, 2004.
- [3] G. Casse, P. Allport, and A. Watson, "Effects of accelerated annealing on p-type silicon micro-strip detectors after very high doses of proton irradiation," *Nucl. Instrum. Meth. A*, vol. 568, pp. 46–50, 2006.
- [4] G. Casse, P. Allport, and A. Greenall, "Response to minimum ionising particles of p-type substrate silicon microstrip detectors irradiated with neutrons to LHC upgrade doses," *Nucl. Instrum. Meth. A*, vol. 581, pp. 318–321, 2007.
- [5] A. Affolder, P. Allport, and G. Casse, "Studies of charge collection efficiencies of planar silicon detectors after doses up to 10^{15} neq cm⁻² and the effect of varying diode configurations and substrate types," *Nucl. Instrum. Meth. A*, vol. 604, pp. 250–253, 2009.
- [6] G. Kramberger, M. Batic, V. Cindro, I. Mandic, M. Mikuz, and M. Zavrtanik, "Annealing studies of effective trapping times in silicon detectors," *Nucl. Instrum. Meth. A*, vol. 571, pp. 608–611, 2007.
- [7] G. Kramberger, V. Cindro, I. Mandic, M. Mikuz, and M. Zavrtanik, "Influence of trapping on silicon microstrip detector design and performance," *IEEE Trans. Nucl. Sci.*, vol. 49, no. 4, pp. 1717–1723, 2002.
- [8] J. Weber and R. Klingenberg, "Free charge carriers trapping properties in neutron-irradiated DOFZ silicon pad detectors," *IEEE Trans. Nucl. Sci.*, vol. 54, no. 6, pp. 2701–2705, 2007.
- [9] L. Rossi, P. Fischer, T. Rohe, and N. Wermes, *Pixel Detectors: From Fundamentals to Applications*. Germany: Springer, 2006.
- [10] L. Evensen, A. Hanneborg, B. S. Avset, and M. Nese, "Guard ring design for high voltage operation of silicon detectors," *Nucl. Instrum. Meth. A*, vol. 337, pp. 44–52, 1993.
- [11] G. A. Beck, A. A. Carter, T. W. Pritchard, J. R. Carter, D. J. Munday, and D. Robinson *et al.*, "Radiation-tolerant breakdown protection of silicon detectors using multiple floating guard rings," *Nucl. Instrum. Meth. A*, vol. 396, pp. 214–227, 1997.
- [12] M. Da Rold, A. Paccagnella, A. Da Re, G. Verzellese, N. Bacchetta, and R. Wheadon *et al.*, "Radiation effects on breakdown characteristics of multiguarded devices," *IEEE Trans. Nucl. Sci.*, vol. 44, no. 3, pp. 721–727, Jun. 1997.
- [13] B. S. Avset and L. Evensen, "The effect of metal field plates on multi-guard structures with floating p+ guard rings," *Nucl. Instrum. Meth. A*, vol. 377, pp. 397–403, 1996.
- [14] M. Da Rold, N. Bacchetta, D. Bisello, A. Paccagnella, G. F. D. Betta, and G. Verzellese *et al.*, "Study of breakdown effects in silicon multi-guard structures," *IEEE Trans. Nucl. Sci.*, vol. 46, no. 4, pp. 1215–1223, Aug. 1999.
- [15] M. Boscardin, L. Bosisio, A. Candelori, G. F. D. Betta, S. Dittongo, and P. Gregori *et al.*, "An improved termination structure for silicon radiation detectors with all p-type multiguard and cut-line implants," *IEEE Trans. Nucl. Sci.*, vol. 50, no. 4, pp. 1001–1007, 2003.
- [16] C. Y. Chien, H. S. Cho, G. W. Liang, X. B. Xie, W. Huang, and Z. Li, "New designs of CMS silicon pixel detectors for radiation hardness," *Nucl. Instrum. Meth. A*, vol. 455, pp. 564–575, 2000.
- [17] M. Benoit, A. Lounis, and N. Dinu, "Simulation of radiation damage effects on planar pixel guard ring structure for ATLAS inner detector upgrade," *IEEE Trans. Nucl. Sci.*, vol. 56, no. 6, pp. 3236–3243, Dec. 2009.
- [18] O. Koybasi, D. Bortoletto, T. E. Hansen, A. Kok, T. A. Hansen, and N. Lietta *et al.*, "Design, simulation, fabrication, and preliminary tests of 3D CMS pixel detectors for the Super-LHC," *IEEE Trans. Nucl. Sci.*, Aug. 2010, to be published.
- [19] "Synopsys TCAD Manuals" Synopsys Inc., 2007 [Online]. Available: <http://www.synopsys.com/products/tcad/tcad.html>
- [20] Y. Okuto and C. R. Crowell, "Threshold energy effect on avalanche breakdown voltage in semiconductor junction," *Solid-State Electronics*, vol. 18, no. 2, pp. 161–168, 1975.
- [21] A. K. Srivastava, A. Bhardwaj, K. Ranjan, Namrata, S. Chatterji, and R. K. Shivpuri, "Two-dimensional breakdown voltage analysis and optimal design of a microstrip detector passivated by a dielectric," *Semicond. Sci. Technol.*, vol. 17, no. 5, pp. 427–434, May 2002.
- [22] H. F. W. Sadrozinski, C. Betancourt, R. Heffern, I. Henderson, J. Pixley, and A. Polyakov *et al.*, "Total dose dependence of oxide charge, interstrip capacitance and breakdown behavior of sLHC prototype silicon strip detectors and test structures of the SMART collaboration," *Nucl. Instrum. Meth. A*, vol. 579, pp. 769–774, 2007.
- [23] M. Petasecca, F. Moscatelli, D. Passeri, and G. U. Pignatelli, "Numerical simulation of radiation damage effects in p-type and n-type FZ silicon detectors," *IEEE Trans. Nucl. Sci.*, vol. 53, no. 5, pp. 2971–2976, 2006.
- [24] D. D. Pitzl, N. Cartiglia, B. Hubbard, J. Leslie, K. O'Shaughnessy, and W. Rowe *et al.*, "Study of radiation effects on AC coupled silicon strip detectors," *Nucl. Phys. Proc. Suppl.*, vol. 23B, pp. 340–346, 1991.
- [25] D. Pennicard, C. Fleta, R. Bates, V. O'Shea, C. Parkes, G. Pellegrini, and N. Tartoni, "Simulations of radiation-damaged 3D detectors for the Super-LHC," *Nucl. Instrum. Meth. A*, vol. 592, pp. 16–25, 2008.
- [26] M. Moll, "Radiation damage in silicon particle detectors—microscopic defects and macroscopic properties," Ph.D. dissertation, Hamburg, 1999.